Nanoscale

Accepted Manuscript

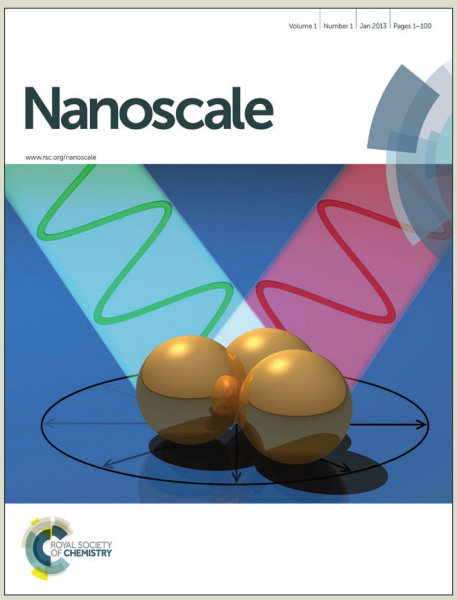

ROYAL SOCIETY OF CHEMISTRY

www.rsc.org/nanoscale

Journal Name

ARTICLE

Self-assembled SnO_2 micro- and nanospheres-based gas sensor thick films from alkoxide-derived high purity aqueous colloid precursor

Received 00th January 20xx,
Accepted 00th January 20xx

DOI: 10.1039/x0xx00000x

www.rsc.org/

G. Kelp[a,b], T. Tätte[a,†], S. Pikker[a], H. Mändar[a], A. G. Rozhin[c], P. Rauwel[d], A. S. Vanetsev[a], A. Gerst[a], M. Merisalu[a], U. Mäeorg[e], M. Natali[f], I. Persson[g], V. G. Kessler[g]

Tin oxide is considered to be one of the most promising semiconductor oxide materials for use as gas sensors. However, simple route for controllable built-up of nanostructured, sufficiently pure, hierarchical SnO_2 structures for gas sensor application is still a challenge. In the current work, an aqueous SnO_2 nanoparticulate precursor sol free of organic contaminants and sorbed ions and fully stable in time was prepared in a highly reproducible manner from an alkoxide $Sn(OR)_4$, just mixing it with large excess of pure neutral water. The precursor is formed as a separate liquid phase. The structure and purity of the precursor is revealed by XRD, SAXS, EXAFS, HRTEM imaging, FTIR, and XRF analyses. An unconventional approach for estimation of the particle size based on quantification of the Sn-Sn contacts in the structure was developed using EXAFS spectroscopy and verified by HRTEM. To construct the sensors with hierarchical 3D structure, we applied an unusual emulsification technique, not involving any additives or surfactants and using simply the extraction of the liquid phase, water, with the help of dry butanol under ambient conditions. The originally generated crystalline but yet highly reactive nanoparticles form relatively uniform spheres by self-assembly and solidify instantly. The spheres floating in the butanol were let to deposit on the surface of quartz plates bearing sputtered gold electrodes, producing ready-for-use gas sensors in the form of ca. 50 µm thick spheres-based-films. The films were dried for 24 h and calcined at 300 ˚C in air before use. The gas sensitivity of the structures was tested in temperature range 150-400 ˚C. The materials showed very quickly emerging and reversible (20-30 times) increased electrical conductivity as a response to exposure to air containing 100 ppm of H_2 or CO and short (10 s) recovery times when gas flow was stopped.

Introduction

The need to detect reducing gases to set alarm for hazards, as a part of technological processing, or for quality control, is arising in domestic or commercial as well as in industrial environments. For this purpose, a huge variety of different gas detection systems made based on metal oxides are proposed. Metal oxide semiconductors are preferable as alteration of their electrical conductivity due to sorption of gases on their surface is rather easy to measure.

Pure SnO_2 is identified as one of the most sensitive systems towards reducing gases. It has attracted a lot of research interest[1] and sensors based on it have been commercially available already for more than 35 years, e.g. Figaro sensors. However, many theoretical as well as engineering related issues are still remaining a challenge for future, and improved sensors are very much requested. A lot of progress should be made, for example, to decrease the working temperature of sensors as close as possible to the ambient environment. It is also an issue to increase selectivity of sensors in order to detect specific gas or gases in a mixture. In addition, advances can be made to make sensors more sensitive, stable in time, cheaper, etc.

For the purpose of electrical sensing, solid state metal oxide sensors, including those based on SnO_2, are mostly proposed to be used in the form of polycrystalline thick films. In such films, electrons will pass from one grain to another by crossing the grain-grain Schottky barrier ensuring the maximum impact of the surface changes onto the concentration of free charge

[a] Institute of Physics, University of Tartu, Ravila 14C, 50411, Tartu, Estonia.
[b] Department of Physics, The University of Texas at Austin, Austin, Texas 78712, USA.
[c] Aston University, Aston Triangle, Birmingham, B4 7ET, UK.
[d] Department of Physics, Centre for Materials Science and Nanotechnology, University of Oslo, PO Box 1048 Blindern, N-0316 Oslo, Norway.
[e] Institute of Chemistry, University of Tartu, Ravila 14A, 50441, Tartu, Estonia.
[f] ICIS-CNR, CorsoStatiUniti 4, 35127 Padova, Italy.
[g] Department of Chemistry and Biotechnology, Swedish University of Agricultural Sciences, P.O. Box 7015, SE-756 51 Uppsala, Sweden.
† Ravila 14c, 50411, Tartu, ESTONIA; tanel.tatte@ut.ee

carriers.[2] The mechanism of conductivity and its sensitivity toward gaseous environment sets up the list of requirements for the sensor materials.

Nanograin material structure is preferred due to its higher sensitivity that enables the use of lower working temperatures and thus save energy. Energy saving is especially important topic as gas sensors are often energized with batteries, which have to be replaced frequently due to discharging. Purity of sensor material is also a huge issue as electrical effects arising from unwanted dopants might be more pronounced than effects caused by gases under detection. For the SnO_2 materials, the problems related to their purity depend on the nature of precursors. Usage of carbon based chemistry leaves the final materials contaminated with considerable amount of carbon entrapped in the structure.[3] Halides, e.g. $SnCl_2$ and $SnCl_4$, give products contaminated with corresponding elements, e.g. Cl^- anions.[4] Last but not least, the design of sensor device should provide enough exposure of sensitive surface to gases under detection; hence, merely a flat film is not the best solution due to the limited surface area. A smart solution would be the use of some complex hierarchical structures like those based on hollow microspheres[5], electrospinning fibres[6] or single-crystalline nanoribbons[7]. Microspheres based structures as thick films of microspheres on isolating substrate are advantageous since they form a network of spheres that are in contact with each other via their surface. Conducting electrons have to jump from sphere to sphere and therefore are forced to pass over active surfaces in contact points of the spheres for many times. It is worth mentioning that apart from the use in sensors,[8,9] SnO_2 microspheres have also been proposed as luminescent material in optoelectronic devices[10] and as anode material in lithium ion batteries[11].

Reports on SnO_2 microsphere preparation utilize hydrothermal[10,12] or solvothermal[13] methods, where microsphere formation is spontaneous[13] or induced by additional chemicals[10] or templates.[12] Other major group of techniques use dense sacrificial spherical templates, e.g. carbon,[14] polymer[9] or nickel[8] microspheres. Removal of the templates is achieved by high temperature calcination or etching.[8] All aforementioned methods can be considered as growth methods, since SnO_2 spheres are assembled from SnO_2 nanoparticles or other intermediate products of chemical reactions. Common sources of tin in these methods are $SnCl_4$ or $SnCl_2$. Thus, the obtained structures are difficult to prepare with high purity as chlorine is known to be difficult to remove because of its high affinity to SnO_2.[15,16]

A different approach for preparation of metal oxide spherical particles is dispersing the precursor liquid into a homogenous phase (gas or liquid) and subsequent solidification of the formed micro- or nanodroplets. Dispersion is obtained by using phase separation or mechanical agitation, including stirring, ultrasonication, jet-injection or spraying – methods that cause break-up of continuous precursor phase into smaller parts. Spherical shape of the particles is achieved due to surface tension of the precursor droplets. The formation and characteristics of droplets are determined by physical and chemical properties of the precursor liquid and medium into which it is introduced.[17] After obtaining spherical shape, the solidification of precursor droplets needs to be achieved. For gaseous media, spray drying[18] is the most common method, where elevated temperature causes solvent evaporation from the spheres. In case of emulsions, solidification is achieved by solvent extraction, evaporation, chemical reaction, etc. However, such methods have rarely been used for preparing SnO_2 spheres.

In this work a thick film architecture composed of nanostructured SnO_2 microspheres was constructed on isolating substrates bearing gold electrodes and was applied for electrical detection of reducing gases: CH_4, H_2 and CO. The spheres as building blocks of the films were prepared from highly pure aqueous SnO_2 nanosol that was emulsified into dry alcohol. Extraction of the liquid phase (water) out from the sol droplets by hydrophilic dry alcohol leads to transformation of droplets into solid gel spheres via sol-gel transition of the SnO_2 sol.

SnO_2 nanocolloidal sol precursor for preparation of the spheres was produced by hydrolysis of tin(IV)alkoxide (e.g. butoxide) by large excess of water under neutral conditions. Formed particles of sol are stable in water supposedly due to the hydrogen bonding via –OH groups on their surface. The precursors are highly pure with concentration of organic additives below detection limit of IR spectroscopy.

Gas sensitivity of electrical conductance of microsphere based films was investigated in the temperature range from 150 to 400 ˚C. Exposure of the sensors to 100 ppm of H_2 as well as CO in air resulted in 20-30 times increased electrical conductance in around 10 seconds time. The sensors showed quick and full recovery over many cycles of usage.

Experimental details

Precursor preparation

Tin(IV)butoxide ($Sn(OBu)_4$), synthesized as described elsewhere,[19] was obtained as transparent brownish yellow sugar-syrup-like viscous liquid. Purity of the obtained alkoxide, in terms of chloride incorporation, could be controlled by adding small quantity of used reactants (diethylamine and butanol) to the filtered alkoxide solution in hydrocarbon solvent before its concentration with evaporator. The reaction is finished when no additional solid sedimentation (diethyl ammonium chloride salt) appears.

For precursor synthesis, 5 g of $Sn(OBu)_4$ was dissolved in 10 g of butanol and then hydrolyzed by pouring the mixture rapidly into 50 g of water. As alkoxides are highly hydrophobic compounds then white voluminous slurry immediately formed at the moment of mixing. During the next 2 h, the slurry dissolved and two separate homogeneous liquid layers formed as a result of phase separation. The upper butanol layer had brown-yellowish hue due to the additives originating from alkoxides. As a result of concentration of butanol layer with Büchi rotational evaporator Rotavapor® R-124, 17 mg of dark brown substance was obtained. For identification of structure

and origin of the additives, an IR spectrum of the obtained substance was recorded (Figure S1).

The lower layer was transparent, almost colorless, aqueous system containing nanocolloidal SnO_2. Obtained sol was purified from brown additives by extracting it 2-3 times with reactant-grade butanol by Sigma-Aldrich®.

To obtain the precursor ready for use in preparation of spheres, the colloidal solution was concentrated on Rotavapor® under vacuum (1-2 torr) at 35-40 °C using water bath until colorless highly viscous sugar syrup-like liquid remained. The concentration process was stopped as soon as solid formations started appearing on the walls of the evaporator bulb.

Precursor analysis

Obtained precursor was analyzed using small angle X-ray scattering (SAXS), extended X-ray absorption fine structure (EXAFS), X-ray powder diffraction (XRD), high-resolution transmission electron microscopy (HRTEM), and infrared (IR) spectroscopy.

SAXS. Colloidal SnO_2 solution in H_2O with concentration from 2 to 10 volume% was sealed into 1.0 mm and 0.5 mm diameter Mark-tubes by Hilgenberg GmbH. SAXS data in the range of scattering vector modulus q = 0.06 – 5.7 nm^{-1} were recorded on a slit collimation camera KRM-1 using Cu K_α radiation and Dectris® Mythen1K 1D pixel detector. Beam path was kept in vacuum at 0.1 mbar. Pre-processing of scattering data (smoothing, scaling, besmearing) was done by using the program AXES.[20] Volume distribution function of scattering particles was calculated by program system NanoSolver (Rigaku).

Infrared (IR) spectra were recorded on Nicolet™ 6700 FT-IR with diamond ATR device, DLaTGS detector and µ-ATR sampling accessory with diamond crystal allowing measurements down to 225 cm^{-1}.

XRD diffraction patterns were recorded with Philips PW3020 Bragg-Brentano powder diffractometer using Cu K_α radiation in 2θ-ω scanning mode. Liquid samples were loaded into Lindeman glass capillaries (0.1 mm wall thickness, 1 mm diameter).

EXAFS data collection. Tin K-edge X-ray absorption data were collected at the Stanford Synchrotron Radiation Light source (SSRL) using the wiggler beam line 4-1, which was equipped with a Si [220] double crystal monochromator. The storage ring was operated at 3.0 GeV, and a current of 297-300 mA. The data collection was performed in transmission mode at ambient temperature, and higher order harmonics were rejected by detuning the second monochromator crystal to 70% of maximum intensity at the end of the scans. Solid tin(IV)oxide was diluted with boron nitride to give an approximate edge step of about one unit in the logarithmic intensity ratio. The aqueous tin(IV)oxide suspension was kept in a cell with 6 µm polyethylene film windows and a 1.5 mm teflon spacer. The X-ray absorption spectra were energy calibrated by means of a simultaneously measured tin foil as internal standard, assigning the first inflection point of the tin K-edge to 29200 eV.[21] The EXAFSPAK program package was used to average four spectra for each sample after energy calibration.[22]

EXAFS data analysis. Further data treatment was performed with EXAFSPAK,[22] with all distances with Gaussian distribution. The EXAFS oscillations were obtained after pre-edge subtraction, normalization and spline removal.[23] Model refinements in EXAFSPAK use ab initio calculated phase and amplitude parameters obtained from the FEFF7 program for single and multiple scattering pathways.[21] Input files to FEFF7 were compiled from the corresponding crystal structures to contain the Cartesian coordinates of all atoms within a 7 Å radius from the tin center.

The standard deviations given for the refined parameters of the model functions are obtained from least squares fit to the k^3 weighted EXAFS oscillations $\chi(k)$, and do not include systematic errors of the measurements. However, the estimated statistical errors allow comparisons e.g., of the relative shifts in the distances. The variations in the refined parameters, using different models and data ranges including the shift in the E_o value (for which k = 0), indicate that the accuracy of the distances obtained for well-defined atom-pair interactions in the complexes is within ±0.01 to 0.02 Å. The estimated errors given in the text have been increased accordingly to include effects of systematic deviations.

HRTEM was performed on JEOL 2010F operating at 200 kV and disposing a point to point resolution of 2 Å. The material was crushed and dispersed in ethanol after sonication. A drop of the suspension was then placed on a holey carbon grid and allowed to dry.

Preparation of microspheres

The SnO_2 spheres were obtained by transforming the aqueous dispersions (generated as described below) of precursor into solid in dry butanol medium. The solidification was achieved as a result of extraction of liquid phase of SnO_2 sol (water), by hydrophilic emulsifying alcohol medium butanol, which can dissolve maximum around 8% of water. Emulsions were generated using 3 different mixing methods. Estimations of diameter and transparency of the spheres were given on the basis of visual assessment from SEM and optical microscopy images respectively.

Ultrasound mixing. 0.1 ml of precursor and 2 ml of dry butanol were taken into a plastic Eppendorf tube so that they formed two separate liquid layers, precursor as denser on the bottom. The liquids were mixed with Diagenode Nanoruptor ultrasonicator for emulsion generation. A sample of structures was prepared at each available mode (S, L1, L2, H) as a result of 5 second sonication.

Mechanical shaking. The liquids were placed into an Eppendorf tube the same way as for ultrasonic mixing experiment. Emulsification was carried out with mixer TopMix FB15012 (Fisher Scientific). Three different mixing rates (800, 1500 and 3000 rpm) were applied.

Injecting into alcohols. A beaker was filled with 10 ml of dry butanol. For emulsion generation 0.1 ml of precursor was injected into the liquid with 1ml insulin syringe in 0.1 seconds.

During injection, the tip of the needle was kept in the liquid phase. Estimated speed of the jet that was pressed through the needle (inner diameter 0.18 mm) was 30-40 m/s.

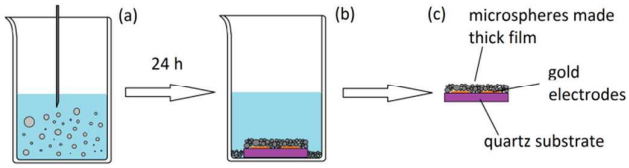

Figure 1 Preparation of SnO_2 microsphere thick film gas sensors. (a) Injection of SnO_2 nanosol into dry butanol for emulsion generation. (b) Solidified SnO_2 microspheres are let to form sedimentation on the surface of a quartz plate with electrodes. (c) Gas sensors ready for use in further experiments.

Gas sensing experiments

To get substrates for electrical gas sensor experiments, 30 nm Au metallic electrode stacks were electron-beam-evaporated on the surface of quartz slides through a shadow mask. Evaporation was carried out at temperature about 300 °C. The electrodes were configured as two parallel few mm wide straight strips distanced with 100 µm gap in between. The substrates bearing the electrodes were placed at the bottom of a glass beaker filled with suspension of spheres in alcohol (the medium they were synthesized in). Overnight the spheres precipitated on the surface of the slides forming a spheres-based thick film coating the electrodes (Fig. 1). The residual liquid was carefully removed by sucking it up via a syringe needle and the substrates were left to dry for additional 24 h.

The samples were heated to 235, 300 and 400 °C for one hour to evaluate the influence of heat treatment on the structure of the formed spheres-based thick films. The surfaces of the films were imaged after the treatment with high-resolution scanning electron microscope system Helios NanoLab 600 (FEI™). Samples used for Raman measurements were heated at 400, 600, 800 and 1000 °C for one hour. Raman spectra of the films were recorded using the Renishaw® in Via µ-Raman spectrometer (spectral resolution 1.5 cm^{-1}). A laser, emitting at 830 nm wavelength, was used for excitation of the samples. About 10 mW of laser power was focused onto 1 μm^2 area using 50x objectives. To detect potential contamination with chloride ions originating from neat compound $SnCl_4$, X-ray fluorescence (XRF) analysis of the obtained films was carried out using Rigaku ZSX 400 spectrometer operating with ZSX Version 5.55 program.

Gas sensor experiments were started by heating the as-prepared samples, aged for 24 h in ambient atmosphere, up to 300 ˚C with a quartz lamp, in a 5 cm^3 stainless steel measuring chamber. Dynamic gas response was evaluated for three reducing gases: H_2, CO and CH_4, balanced with dry 5.0 synthetic air (20 volume% of O_2 in N_2). Experiments were done also using synthetic atmosphere for balancing. 100 ppm of H_2, CO and CH_4 gases were applied in sets, containing two 2.5 minute long cycles. The measurement chamber was purged with synthetic air for 2.5 minutes between the cycles. A constant total gas flow of 300 cm^3/min was maintained during the measurements. Sensing behaviour of the samples was investigated by recording the changes in the electrical current *I* through the films introduced to different gas environments. The response of the sensor was defined as the ratio I/I_0, where I_0 marks the base level current, i.e. the current before the application of gas. In order to avoid structural changes that could be caused by electrical current, low 1 V voltage was constantly applied to the films throughout the all experiments using Keithley 2400 SourceMeter®. Electrical current was detected at the same time with the same instrument. Measurements were carried out at 400, 300, 200, and 150 °C.

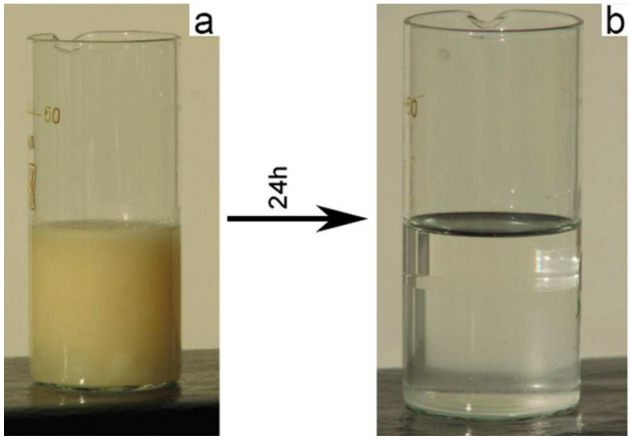

Figure 2 Preparation of the aqueous SnO_2 sol. (a) The slurry-like mixture of $Sn(OBu)_4$ and water right after their mixing. (b) The separated colorless layers of butanol and SnO_2 aqueous nanosol. The reaction of alkoxide with water is complete, the phases are separated and brown additive is fully removed by 3 times extraction with alcohol

The maximum error in determining gas sensors response I/I_0 under apply of certain conditions is evaluated to be less than 5% and it includes error of direct electrical measurements, gas composition error (equipment by AGA, error up to 2%) and temperature measurement error. As gases were kept the same and no modifications were done to the experimental set-up throughout the measurements, then relative error appearing from experiment to experiment was probably even lower. Due to the low applied voltage (1 V) and low currents in the devices, additional heating is negligible and no structural changes resulting from that are expected or observed.

Results and discussion

Preparation of stable aqueous SnO_2 sols under neutral conditions.

After pouring $Sn(OBu)_4$, diluted with butanol, into water for hydrolysis, a slurry-like mixture of two mutually insoluble liquids (water and alkoxide) formed immediately (Figure 2a). The structure of hydrolyzing alkoxide can be expressed as $SnO_x(OH)_y(OR)_z \cdot wH_2O$. As the hydrolysis reaction proceeds, -OR groups are substituted by much more hydrophilic –OH groups and oxo-ligands. Finally, all alkoxide is transformed into aqueous SnO_2 nanoparticulate sol and alcohol. The latter

forms a layer on the top of aqueous sol as a result of phase separation.

Historically, the hydrolysis of tin compounds has been described to lead to the formation of stannic acids, first forming transparent solutions (α-stannic acid) that transform later into opaque colloid (β-stannic acid).[24] It has been considered that the α-form is bearing mostly OH-groups, while the β-form is rich in oxo-ligands. Development of the modern insight into general principles of colloid chemistry resulted in the abandonment of the terms α- and β-stannic acids in the late 1970s.

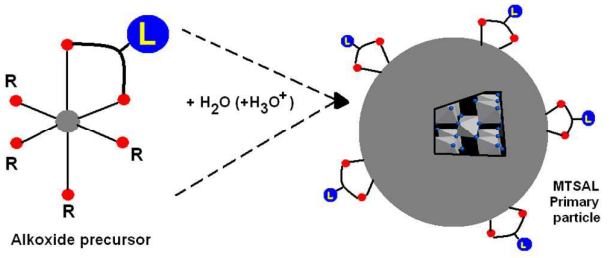

Figure 3 Formation of a MTSAL polyoxometallate nanoparticle during hydrolysis of an alkoxide precursor (*L* stands for ligand). The image is reprinted with permission from ref. 25.

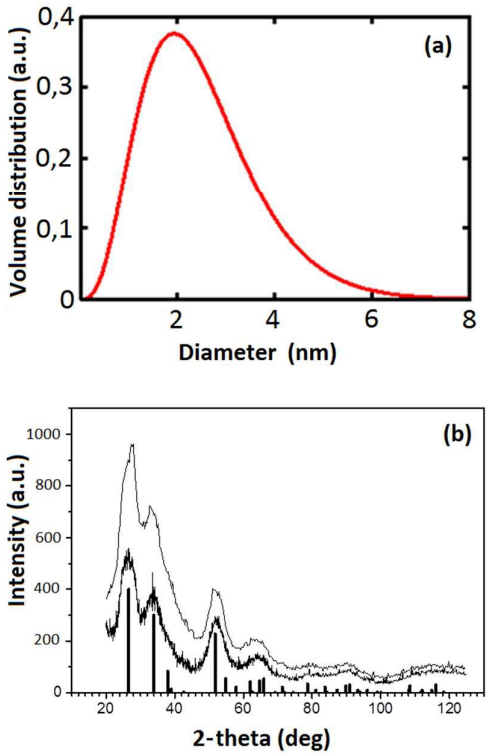

Figure 4 (a) SAXS determined particle size distribution function for spherical particles of SnO_2 in H_2O. (b) XRD 2θ-ω scans of liquid nanoparticle suspension (upper) and xerogel obtained by drying the suspension at room temperature in air for 7 days (lower). Vertical bars represent relative intensities of the powder diffraction reference pattern ICDD 41-1445 of tetragonal cassiterite SnO_2 phase.

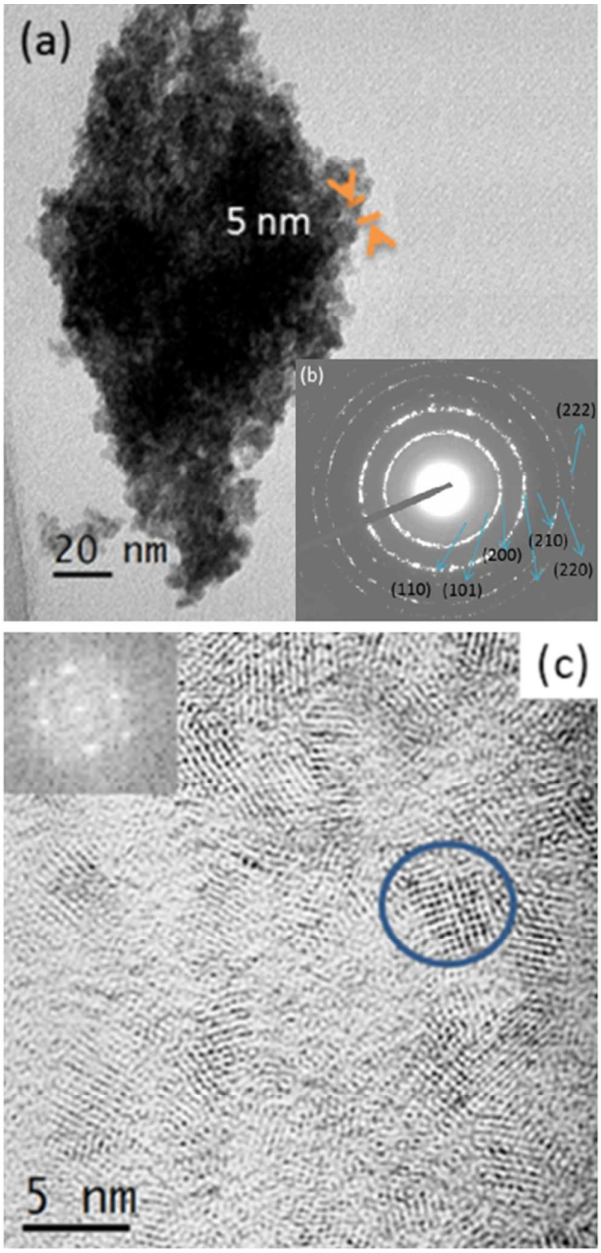

Figure 5 (a) Low resolution image of an agglomerate of SnO_2 nanoparticles. (b) SAED pattern of (a). (c) HRTEM image of (a), inset is the FFT of the encircled particle.

A reasonable explanation for the phenomena is that the tin oxide phase is emerging first in the form of small nuclei with high surface area and very considerable degree of surface hydration. As the reaction continues, these small primary particles aggregate and coalesce, decreasing the exposed surface and hydration degree and becoming visible through light scattering (opalescence) as their size approaches the wavelength of visible light.

The nucleation of metal oxide phase occurs generally in the form of near-spherical shape oxometallate species 2-5 nm in size that behave as colloid particles due to their size (Figure 3).[25] These particles are nowadays denoted as Micelles Templated by Self-Assembly of Ligands (MTSALs) in the view of their origin in coordination equilibrium (self-assembly) and analogy with micelles.[26,27] The cores of MTSALs are consisting of densely packed metal cations and oxide anions mimicking thus the structure of the thermodynamically most stable relevant metal oxide, while the shells are amorphous and contain residual ligands other than oxide (organic, hydroxide and water molecules). The structure of the core is essentially the same regardless of the nature of applied precursor, while the structure, thickness and charging of the shell are very much dependent on the nature of potentially present ligands and pH in the solution. As SnO_2 colloids are most often produced from the individual coordination compound $SnCl_4 \cdot 5H_2O$ (CAS No 0010026069), containing cis-$SnCl_4(H_2O)_2$ units,[28] on action of relatively concentrated ammonia, the nucleation occurs there in a basic medium (pH 9.5 or higher) and is associated apparently with formation of negatively charged MTSALs. Their cores are composed of cassiterite phase, just as in the present work, but the shells are relatively thin and the particles easily aggregate on transition to neutral pH through charge compensation.[29] This is a problem when sols are prepared in order to use for technological purposes, e.g. synthesis of SnO_2. More stable compounds would be prepared under neutral conditions, like it is done in current study where neutral alkoxide is just mixed with water.

SAXS analysis of the size and shape of obtained SnO_2 sols demonstrated the weakest concentration effect on the scattering curve at concentrations of 2 and 5 volume% (in H_2O), which for these samples were used in the further analysis. Assuming a spherical shape, the estimated average diameter of the obtained particles was 2.5(3) nm, with dispersion of about 48% (Figure 4a). Model calculations for a rod-shape particle gave a worse match with experimental scattering data. Therefore, most probably the primary SnO_2 particles in the precursor have a spherical or close to spherical isotropic shape.

It can also be seen from Fig. 5 that the shells of the particles produced from alkoxide precursors are apparently thick, which is resulting in lower degree of crystallinity, but also in the possibility of stabilization for dispersions simply via hydrogen bonding between the particle shells and water molecules. The same was revealed also by EXAFS analysis, which showed that tin atoms in the system are almost equally divided into metal oxide-like cores and amorphous shells.

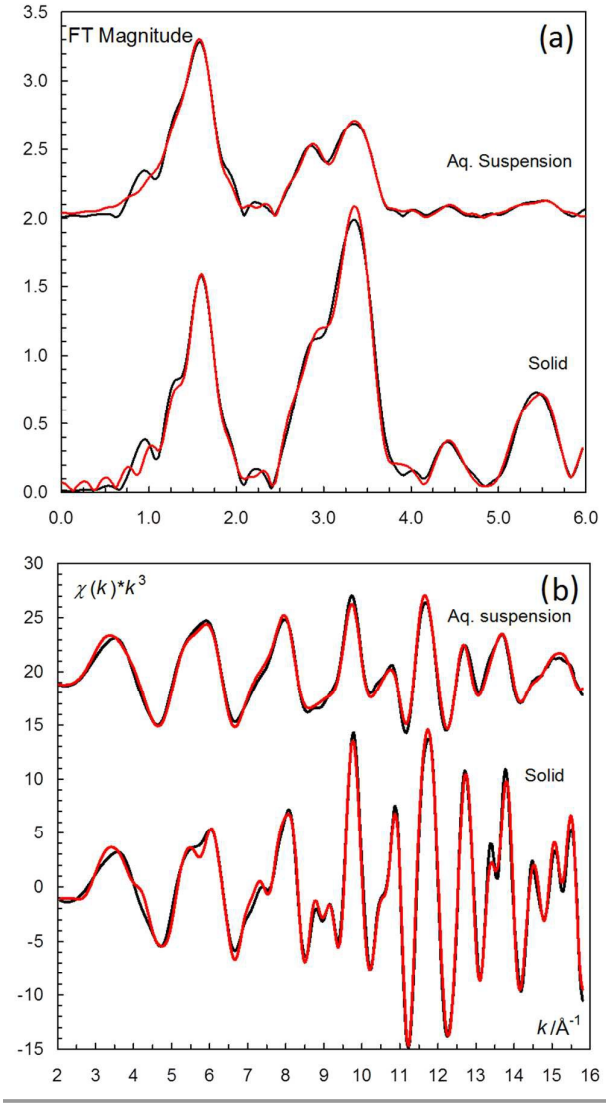

Figure 6 (a) Fit of the Fourier transforms of EXAFS data for solid tin(IV)oxide and aqueous suspension of nano-sized colloidal tin(IV)oxide particles; black line – experimental data, and red line – model. Data lines are vertically shifted for clarity. (b) Fit of k^3-weighted EXAFS data of solid tin(IV)oxide and aqueous suspension of nano-sized colloidal tin(IV)oxide particles; black line – experimental data, and red line – model. Data lines are vertically shifted for clarity.

The Fourier transforms from the EXAFS data of solid tin(IV)oxide and the aqueous stannic acid suspension display very similar distances (Figure 6a). The size of the peak corresponding to Sn-O bonds is the same in both samples, while the number of Sn···Sn distances is much smaller in the aqueous suspension (Figure 6a, Table 1). Furthermore, there are hardly any Sn···Sn distances observed beyond 6 Å.

	Solid SnO_2		Solid SnO_2			Aq. suspension of SnO_2		
	XRD		EXAFS			EXAFS		
Distance	*d*	*n*	*d*	σ^2	*n*	*d*	σ^2	*n*
Sn-O	2.050	6	2.051(2)	0.0026(2)	6	2.049(2)	0.0040(1)	6
Sn-O	3.594	4	3.52(3)	0.008(3)	4	3.54(3)	0.013(3)	4
Sn···Sn	3.187	2	3.198(2)	0.0021(1)	2	3.207(2)	0.0021	0.81(5)
Sn···Sn	3.710	8	3.720(5)	0.0043(2)	8	3.733(3)	0.0043	2.9(1)
Sn···Sn	4.738	4	4.752(8)	0.0058(3)	4	4.760(14)	0.0058	1.9(3)
Sn···Sn	5.710	8	5.688(7)	0.0077(3)	8	5.675(14)	0.0077	2.6(5)
Sn···Sn	5.837	8	5.908(7)	0.0090(3)	8	5.932(12)	0.0090	2.8(3)

Table 1. Structure parameters, distance, *d*/Å; Debye-Waller coefficient, σ^2/Å^2; and number of distances, *n*, of solid tin(IV)oxide as determined by X-ray crystallography[30,31,32,33,34] and EXAFS, and aqueous suspension of colloidal tin(IV)oxide by EXAFS.

This shows that solid tin(IV)oxide and the aqueous suspension of colloidal tin(IV)oxide have the very same structure, but due to the small size of the colloidal particles the number of Sn···Sn distances will be reduced. The refinement of the structure parameters of solid tin(IV)oxide showed that they were in excellent agreement with previously reported crystal structures (Table 1). Fit of the EXAFS data is given in Figure 6b. The obtained Debye-Waller factors in solid tin(IV)oxide were then used as fixed parameters to determine the number of Sn···Sn distances in the aqueous suspension. It is important to stress that the correlation between the Debye-Waller factor and the number of distances is very strong, and these parameters cannot be refined simultaneously. The obtained bond distances and number of the various Sn···Sn distances in solid SnO_2 and the stannic acid aqueous suspension containing nano-sized SnO_2 particles as determined by EXAFS are summarized in Table 1 together with the same parameters from crystallographic studies.

In order to estimate the mean size of the colloidal SnO_2 particles, the number of Sn···Sn distances at 3.2, 3.7 and 4.7 Å was calculated for some particle sizes based on the structure of the solid SnO_2 (cassiterite phase with rutile structure). The obtained number of Sn···Sn distances in a particle consisting of 45 unit cells (three unit cells along the a and b axes and five along the c axis) gave a particle approximately 2x2x2 nm in size assuming that oxygen atoms are facing the aqueous solution. Such a particle will have 1.08, 3.83 and 2.89 Sn···Sn distances per Sn at 3.2, 3.7 and 4.7 Å, respectively. Assuming a spherical particle with a diameter of 2 nm will give ca. 74% of the number of Sn···Sn distances in almost cubic particle, 0.80, 2.83 and 2.14 Sn···Sn distances per Sn at 3.2, 3.7 and 4.7 Å, respectively. This fits very nicely with the experimentally observed ones, 0.8, 2.9 and 1.9 (Table 1), strongly supporting the observations made by SAXS. This result also correlates quite well with the HRTEM observations (Fig. 5c), indicating that the applied unconventional EXAFS-data based analysis of metal atom coordination provides a valuable tool for determination of the average size of primary particles (MTSALs) when generated in solution. This makes EXAFS in parallel with SAXS a tool for in situ inspection of the size and the structure of the emerging nuclei.

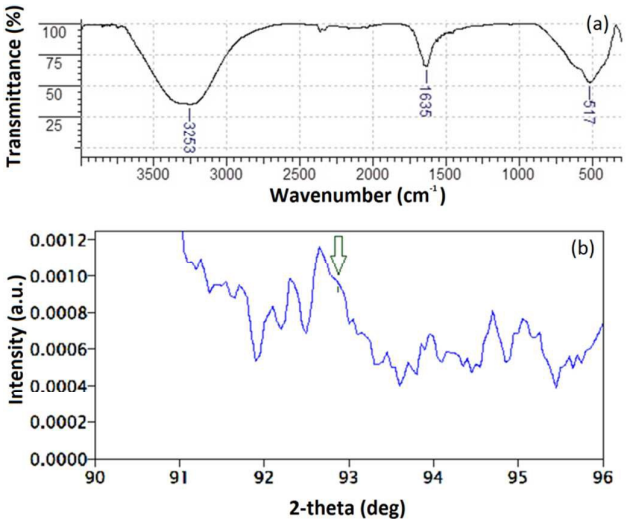

Figure 7 Purity of particles. (a) FTIR spectra of aqueous SnO_2 nanosol. (b) X-ray fluorescence analysis spectrum of SnO_2 spheres in the region of Cl-KA (marked by arrow) presents only background noise.

In fact, the EXAFS spectroscopy brings in principal advantages in the investigation of small nanoparticles. This technique is directly structure sensitive and non-invasive, permitting to follow the nucleation and crystal growth from molecular to nano level directly in solution, not requiring phase separation and drying in contrast to, for example, TEM. In addition, it is a low energy density technique compared to high resolution TEM and can, as demonstrated, provide unbiased insight into the crystallinity and size of the emerging particles. Its sensitivity to the short range structure is principally higher than that of the XRD that requires the particles to possess coherence domains of at least several nanometers to make the structure detectable. The emerging crystal structure has been demonstrated by EXAFS for, in particular TiO_2 samples that appeared completely amorphous by X-ray diffraction.[35] It is important to notice that the development of high throughput synchrotron facilities throughout Europe, offering free-of-charge access, in particular, MAX-IV in Lund, Sweden and ESRF in Grenoble, will within just in a couple of years from now make EXAFS in practice an easier accessible technique than high resolution TEM.

Crystallinity of the nanoparticles was determined by XRD analysis (Figure 4b), which revealed cassiterite crystalline SnO_2 phase for both the liquid sample (nanoparticle suspension) and the xerogel sample obtained after aging SnO_2 aqueous precursor for 7 days under ambient conditions with no heat treatment.

The explanation of only partial crystallization in studied nanocolloidal system could also be given from thermodynamic point of view. Though crystallization itself is energetically favorable process in such systems, it is significantly hampered by visco-elasticity of the media. The relation between quantities of crystallized and amorphous phases depends on the quantity of water and alcohol molecules, which are

required to stabilize Sn^{4+} ions in amorphous phase. Thus, the higher the temperature and/or the longer the duration of evaporation process, the higher will be the content of crystalline SnO_2. Although it is worth noting that visco-elasticity will also increase and therefore, due to the well-known equation for energy of formation of nucleus of critical size (Eq. 1) in classical Gibbs-Volmer theory[36], crystallization process will also be hampered.

$$\Delta G^* = \frac{16\pi\sigma^3}{3(G_v)^2} \quad (1)$$

where σ is the coefficient of surface tension and G_v is the difference in free energy per unit volume.

This allows suggesting that on every step of the evaporation process local equilibrium between crystalline and amorphous state is achieved. As usual for such systems, due to three-order dependence of free energy of critical size nucleus formation on viscosity, crystallization runs faster on the earlier stages of process and as visco-elasticity grows, crystallization speed decreases. On the other hand the velocity of growth of formed crystalline particles also decreases due to slowing down of diffusion. Reasonable result of these factors is the formation of highly elastic gel, made of nano-sized crystalline particles that are surrounded by amorphous media.

Purity of prepared sols was studied with IR spectral analysis. Obtained spectra contained no peaks that could be attributed to organic groups (Figure 7a). The broad band in the spectrum with maximum at 3253 cm^{-1} could be attributed to stretching of O-H bond of water molecules or those linked covalently with Sn atoms. The vibration maximum at 1635 cm^{-1} corresponds to the bending mode of water and/or Sn-O-H with hydrogen-bonded water. Vibration maximums in the region of 400 to 600 cm^{-1} correspond to the stretching of Sn-O bond.[37,38] The obtained material had strong complex absorption at 517 cm^{-1} with a shoulder at 638 cm^{-1}, which could be attributed to Sn-O stretching mode. The specific absorption for nanosized tin oxide surface is reported at 564 cm^{-1}, the value dependent on the shape and size of the particles. This absorption could also be present in a complex broad absorption band in the region 530-620 cm^{-1}.[37] Two strong signals at 656 and 556 cm^{-1} were treated in literature as indicators of good crystallinity of the SnO_2 nano-material obtained by hydrothermal treatment.[38] The material prepared in the present investigation does not have any substantial absorption at 656 cm^{-1}, which could be considered as an indication of relatively low content of small crystals.

The use of alkoxides in the preparation of aqueous SnO_2 sols also enables to solve problems related to material purity in terms of chloride ions which are especially troublesome as their presence would effectively increase electrical conductance of the final material and therefore lower the sensitivity of sensors. Namely, it would be difficult to distinguish the increase of conductivity as a response to gases when material itself is already a good conductor because of bulk doping.[39] As removal of chlorine from final materials is a complicated task[3,15,16] due to its high affinity toward oxides then it is smart to solve the problem by removing it in earlier stages. It can be done during the synthesis of alkoxide by bonding released chlorine effectively to diethylammonium complex that forms voluminous sedimentation and can be fully filtered out. The experiments showed that if even a small amount of chlorine remains in the synthesized alkoxide, the synthesis conditions of SnO_2 sol are acidic and SnO_2 forms as solid sedimentation and not homogeneous sol. Therefore we propose to check the completeness of alkoxide synthesis reaction by adding a small amount of alcohol and diethylamine to the alkoxide before use. If any sediment forms, it should be filtered out. XRF analysis of final sensor materials (data provided in the next section) proved no detectable amount of chlorine in their content.

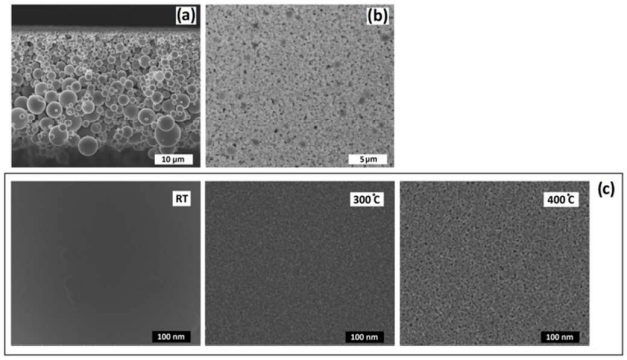

Figure 8 (a) Image of cross-section of SnO_2 spheres-based thick film peeled from substrate surface. (b) Surface of the spheres based film. (c) High resolution SEM images of the surface of approximately 10 micron diameter SnO_2 microsphere before (room temperature, RT) and after heat treatment for 1 h at 300 °C and 400 °C. Morphology changes caused by the treatment can be observed from the images.

Temperature	Peak A_{1g}*	Peak B_{2g}**	Peak E_g	Estimated size
RT	NA	782.3	NA	Amorphous
400 °C	635	777.0	477.8	15*-30** nm
600 °C	635.9	777.9	477.8	25*-40** nm
800 °C	636.9	778.8	477.8	30*-60** nm
1000 °C	636.9	778.8	477.8	30*-60** nm

Table 2 Size estimations of nanocrystallites in microsphere samples heat-treated at different temperatures. Shifts of A_{1g} and B_{2g} vibrational bands were compared with previous data from Diéguez et al.[40] Estimated sizes marked with (*) were obtained by comparing A_{1g} vibrational mode frequencies and sizes marked with (**) were obtained from B_{2g} mode. Although the estimated sizes are imprecise, a trend of crystallite growth can be seen. In contrast to Diéguez et al., we did not see noticeable shifting of the E_g band possibly due to a relatively low spectral resolution 1.5 cm^{-1} of the spectrometer and the small crystallite size sensitivity of the E_g band.

Major difficulty in using aqueous approaches to SnO_2 sensor materials is as stated above the incorporation of inorganic anions (most commonly, Cl^-), leading to principal loss of sensitivity. The alkoxide-based sol-gel approach is characterized by high purity of produced materials due to the possibility of high grade purification of the metal-organic alkoxide precursors.[41] Major challenge in the use of alkoxide precursors is, however, their sensitivity to hydrolysis, making their handling difficult and the reproducibility of the produced materials limited. The present work, demonstrating a facile and quantitative transformation of an alkoxide into an aqueous colloid precursor, demonstrates thus a principally

advantageous and performant approach to fully reproducible and highly pure SnO_2 nanomaterials.

SnO_2 spheres-based thick films for gas sensors

The tin dioxide sensor materials remain a truly hot and highly addressed topic. In spite of some other more complex and costly materials being proposed recently, SnO_2 remains the major object of studies due to its accessibility and outstanding electro physical properties. Major challenge in application of SnO_2 nanomaterials is the need to provide them with enhanced thermal and chemical stability intimately connected with the quest for high crystallinity. The alkoxide based sol-gel approach has recently been demonstrated to be capable to offer highly crystalline and stable SnO_2 nanostructures when the hydrothermal conditions are applied.[42] In the present work we have demonstrated for the first time that highly crystalline SnO_2 nanomaterial can be produced by facile self-assembly processes, an emulsion synthesis, at room temperature.

The conditions of emulsion generation (mixing of SnO_2 sol and dry butanol) have high impact on the size distribution of the resulting SnO_2 spheres. Ultrasonication based mixing resulted in spheres up to 30 µm in diameter, while the sizes of the smallest spheres remained below 10 nm. Mechanical shaking resulted in the formation of spheres with 2-200 µm diameters and injection mixing in diameters 0.5-10 µm. The primary particles are confined in the emulsion droplets at form spherical aggregates that instantaneously solidify at ambient conditions. This approach is thus very facile, not requiring application of surfactants or solvothermal conditions. While injection has been described earlier for generation of microspheres[43], the solvent extraction has to the best of our knowledge not been used for this purpose earlier.

The proposed design of the sensor elements was preferred because of its simplicity – the floating spheres simply sediment from the liquid phase and form a thick layer on the substrate (quartz plate with two Au electrodes). Residual liquid phase is easy to remove with syringe or by decantation. Images of the film peeled from the surface are presented on Figure 8(a,b). Bigger and heavier spheres precipitate faster to the substrate, creating a size gradient of spheres in the final film, as can be easily seen from the cross-section of the film on Figure 8a.

As SnO_2 gas sensors function at elevated temperatures, the influence of heat-treatment on morphology of the obtained films was studied with SEM and µ-Raman spectroscopy. Optical and SEM imaging showed transparency and nano-scale homogeneity of as-prepared spheres, respectively. SEM characterization of heat-treated samples showed clear morphological changes, most notably after heating at 400 °C. Formed crystallites on the surface of the spheres can be recognized visually from the images (Figure 8c). This result is in good agreement with previous studies.[14]

The crystallization of the samples during heat-treatment was confirmed also by Raman measurements (Figure 9). The Raman spectrum of unheated materials has a broad peak at around 580 cm^{-1} and a broad low intensity peak around 780 cm^{-1}, which could be attributed to a B_{2g} vibrational mode of SnO_2.

Such spectrum proves that unheated samples are composed of material that is mostly amorphous according to Raman measurements.[44] Crystallite growth at annealing was studied as described in ref. 40, and the results are presented in Table 2. Two Raman active bands (A_{1g} and B_{2g}) were compared to each other and using fitted theoretical curves based on the data of Diéguez *et al.*, the size estimations were made.

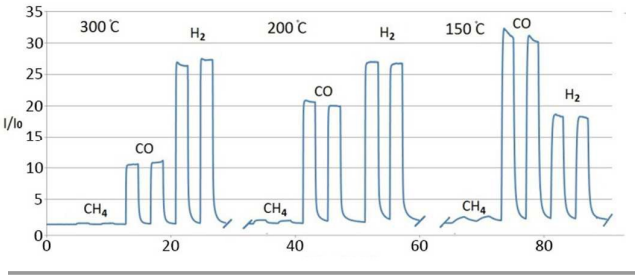

Figure 9 Step response of ratio of electrical current (I) in SnO_2 film placed to synthetic air environment containing 100 ppm of reducing gases (CH_4, CO and H_2) to electrical current (I_0) in the film placed to pure synthetic air environment at corresponding temperature. Constant 1 V potential was applied between the electrodes throughout the experiment. Measurements were carried out at 300, 200, and 150 °C.

A general trend of crystallite size growth can be seen: at 400 °C the crystallites are 15 nm in size, whereas at 1000 °C they grow up to 60 nm. The spectrum of as-prepared samples also contains some low intensity Raman bands at 1463 cm^{-1}, 1060 cm^{-1}, 880 cm^{-1} and 849 cm^{-1}, which can be attributed to butanol originating from spheres preparation. Butanol peaks are lost during the heat-treatment.

After heat treatment the Raman bands typical for SnO_2 with rutile crystal structure arise. The peaks at 637 cm^{-1}, 478 cm^{-1} and 779 cm^{-1} can be assigned to the A_{1g}, E_g and B_{2g} vibrational modes of tetragonal SnO_2.[10,45,46,47,48] The very low intensity peak at 698 cm^{-1} originates possibly from the A_{2u}(LO) mode.[41,45] Another low intensity peak at 546 cm^{-1} is near the amorphous SnO_2 peak at 566 cm^{-1} as reported previously.[41] Minor bands at about 252 cm^{-1}, 304 cm^{-1} and 356 cm^{-1} can also be noticed, which seem to correlate with the IR active E_u(TO) and E_u(LO) modes measured previously elsewhere.[42,43,44] The presence of these modes in the spectra suggests a relaxation of the q = 0 Raman selection rules.[45]

X-ray fluorescence analysis spectrum (Figure 7b), demonstrates that chlorine content, potentially originating from neat compound $SnCl_4$, in as-prepared materials aged for 24h, but not yet heat-treated, remains below detection limit of the method for chlorine (0,08 µg/cm^2).

SnO_2 microspheres-based thick film electrical gas sensors

Step response of electrical current I through the films at 1 V of constant voltage was measured for 100 ppm of CH_4, CO and H_2 pulsing in dry synthetic air respectively (Figure 9). Heating up the as-prepared films (aged for 24h at room temperature) to 300 ˚C resulted in increase of I from 0.01 to 10 nA. Before the measurements, the films were let to stabilize morphologically and electrically at 300 ˚C until stable electrical response was reached. The response of I at 300 ˚C was highest for H_2 (I/I_0=26, where I_0 marks the current before the application of

gas), a bit more than two times lower for CO (I/I_0=11) and close to detection limit in case of CH_4. The sensor displays quite short 10 s rise and decay times for CO and H_2. When sensor temperature was lowered to 150 ˚C then response for gases still remained high. However, absolute values of *I* lowered almost an order of magnitude and the response for CO was more than two times higher compared to H_2. The latter gives an option for selective detection of these gases when responses at different temperatures are compared to each other. The observed decrease in sensitivity to H_2 at lower temperatures in contrast to almost constant absolute value of *I* from adsorbed CO molecules may be explained by different mechanism of signal generation. H_2 molecules tend to reduce surface oxygen atoms and decrease the space charge layer thickness around SnO_2 grains.[49] On the other hand, the signal from CO molecules originates from the substantial donation of charge[50] from CO (Lewis base) to the Sn^{4+} cation (Lewis acid), which increases the surface conductance. Oxidation-reduction process unsurprisingly requires higher temperature to evolve, while charge donation is almost insensitive to such minor changes of ambient temperature.

The sensors started to respond to CH_4 (I/I_0=11) only when they were heated up to 400 ˚C (due to the same reason as for H_2 the response was increasing with the increase in temperature). Unfortunately, heating up to 400 ˚C caused critical morphological changes in the films, which made their further use at lower temperatures (150 and 200 ˚C) no longer possible. However, high I/I_0 values and quick step response of the sensors at 150 ˚C are rare, as in majority of works SnO_2 sensors are used in 300-500 ˚C temperature range, including those grown by ALD,[51] ion beam deposited[52] and screen printed,[53] with gas sensing experiments carried out at 450 °C, 250-400 °C, and 250 °C and more, respectively. Higher sensitivity of microspheres based thick-film gas sensors may be explained by the peculiarities of their structure, namely massive number of sphere-to-sphere contacts, which allow conducting electrons to jump from sphere to sphere and therefore pass active surfaces in contact points of the spheres. In addition, the activity is related to nanostructured surface of the spheres, achieved by preparing them from SnO_2 nanosols. Stable sharp step-response is probably related to high purity of used materials, eliminating the post effects of residues on the current.

Each sensor went initially through 20-30 cycles of measurements. Further temporal stability of the sensors was evaluated by repeating the measurements after 2 months. The difference in I/I_0 response of the sensor was within 5% of the original measurements. More importantly the shape of the response curve remained the same, showing stability and usability of the sensor over elongated periods of time.

Conclusions

In the current study, a robust process is proposed for preparing SnO_2 microsphere-based thick film gas sensors for detection of reducing gases like CO, H_2 and CH_4. The spheres are prepared from high purity aqueous SnO_2 nanocolloidal precursor sols obtained from tin alkoxides under neutral conditions. It was shown by SAXS and EXAFS and confirmed by HR-TEM analysis that the structure of sols is based on spherical-shape tetragonal phase SnO_2 nanocrystallites with mean diameter of about 2-3 nm. EXAFS analysis as well as HR-TEM demonstrated clearly that particles are surrounded by relatively thick amorphous shells, which enables their stability in water for at least many years. The proposed precursors are free of additives as revealed by IR spectroscopy and XRF analysis and therefore provide an excellent basis for high purity nanostructured SnO_2 materials preparation. The formation and stability of sol particles is in good agreement with MTSAL concept. SnO_2 microspheres were prepared by an innovative approach, emulsifying the sol into dry butanol by using different methods and subsequent solidification of the liquid droplets by extraction of liquid phase out of them with the help of dry butanol.

In order to prepare corresponding films, the spheres in solution were left to precipitate on glass substrates equipped with gold electrodes. The films were aged and thermally treated before gas sensing experiments. The current response (I/I_0) at 300 ˚C was highest (26) for H_2, a bit more than two times lower (11) for CO and close to detection limit in case of CH_4. The sensor displayed quite short 10 s rise and decay times for CO and H_2. When sensor temperature was lowered to 150 ˚C, the absolute values of *I* lowered almost an order of magnitude; however, response for gases still remained high. At 150 ˚C the signal from CO was around two times higher compared to H_2. This gives an option for selective detection of these gases when responses at different temperatures are compared to each other. The sensor started to respond to CH_4 (I/I_0=11) when heated up to 400 ˚C. High sensitivity of microspheres-based thick film gas sensors can be explained by their spheres-based structure: large number of contact points between spheres allows conducting electrons to pass through active surfaces at these contact points.

Acknowledgements

This work was supported by Estonian Research Council research targeted projects ETF9292, PUT170, IUT2-24, IUT20-17, and ETF9283; Estonian Centres of Excellences in Research Projects TK117, TK114, and MOBILITAS Top Researcher Grant MTT50; SA Archimedes project 3.2.0304.12-0397 "Nanomaterials - research and applications" (NAMUR). The support from the Swedish Research Council to the project 2014-3938 is gratefully acknowledged. The authors would like to thank A. Kasikov for help in evaporating gold films onto the samples and P. Ritslaid for XRF data.

Notes and references

‡ Supporting Information. IR spectrum of additives found in residual butanol layer formed during precursor preparation.
§ Author Contributions

The manuscript was written through contributions of all authors. All authors have given approval to the final version of the manuscript.

§§ Funding Sources
This work was supported by Estonian Research Council research targeted projects ETF9292, PUT170, IUT2-24, IUT20-17, and ETF9283; Estonian Centres of Excellences in Research Projects TK117, TK114, and MOBILITAS Top Researcher Grant MTT50; SA Archimedes project 3.2.0304.12-0397 "Nanomaterials - research and applications" (NAMUR). The support from the Swedish Research Council to the project 2014-3938 is gratefully acknowledged.

1 N. Barsan, M. Schweizer-Berberich and W. Göpel, *J. Anal. Chem.,* 1999, **365**, 287.
2 N. Barsan, M. Hübner and U. Weimar, *Sensors and Actuators B. Chemical*, 2011, **157**, 510.
3 K. C. Molloy, *J. Chem. Res.,* 2008, 549.
4 A. Hamd, E. Boulle, R. Thune and J. Guinebretiere, *Sol-Gel Sci. Technol.*, 2010, **55**, 15.
5 H. Jiang, J. Hu, F. Gu, W. Shao and C. Li, *Chem. Commun.*, 2009, **24**, 3618.
6 J. Moon, J.-A. Park, S.-J. Lee, T. Zyung and I.-D. Kim, *Sensors and Actuators B*, 2010, **149(1)**, 301.
7 A. Maiti, J. A. Rodriguez, M. Law, P. Kung, J.R. McKinney and P. Yang, P. *Nano Letters*, 2003, **3(8)**, 1025.
8 H.-R. Kim, K.-I Choi, K.-M. Kim, I.-D. Kim, G. Cao and J.-H. Lee, *Chem. Commun.*, 2010, **46**, 5061.
9 C. J. Martinez, B. Hockey, C. B. Montgomery and S. Semancik, *Langmuir*, 2005, **21**, 7937.
10 Y. Han, X. Wu, G. Shen, B. Dierre, L. Gong, F. Qu, Y. Bando, T. Sekiguchi, F. Filippo and D. Golberg, *J. Phys. Chem. C,* 2010, **114**, 8235.
11 S. Han, B. Jang, T. Kim, S. Oha and T. Hyeon, *Adv. Funct. Mater.*, 2005, **15**, 1845.
12 X. W. Lou, C. Yuan and L. A. Archer, *Small*, 2007, **3**, 261.
13 Y. Wang, and T. Chen, *Electrochim. Acta*, 2009, **54**, 3510.
14 Y. Wang, F. Su, J. W. Lee and X. S. Zhao, *Chem. Mater.,* 2006, **18**, 1347.
15 S. M. Ahmed and D. Maksimov, *Journal of Colloid and Interface Science*, 1969, **29(1)**, 97.
16 D. M. Sherman, K. V. Ragnarsdottir, E. H. Oelkers and C. R. Collins, *Chemical Geology*, 2000, **167**, 169.
17 S. Freitas, H. P. Merkle and B. Gander, *J. Controlled Release*, 2005, **102**, 313.
18 S. Lyonnard, J. R. Bartlett, E. Sizgek, K. S. Finnie, Th. Zemb, and J. L. Woolfrey, *Langmuir*, 2002, **18**, 10386.
19 I. M. Thomas, **US3946056**, Mar 23, 1976.
20 H. Mändar, J. Felsche, V. Mikli and T. Vajakas, *J. Appl. Crystallogr.,* 1999, **32**, 345.
21 S. I. Zabinsky, J. J. Rehr, A. Ankudinov, R. C. Albers nad M. Eller, *J. Phys. Rev. B: Condens. Matter Mater. Phys.,* 1995, **52**, 2995.
22 G. N. George and I. J. Pickering, EXAFSPAK - A Suite of Computer Programs for Analysis of X-Ray Absorption Spectra, *SSRL: Stanford, CA.*, 1993.
23 E. D. Crozier, J. J. Rehr and R. Ingalls, R. In X-Ray Absorption, Principles, Applications, Techniques of EXAFS, SEXAFS, and XANES, *Chapter 9; Koningsberger, D.C. and Prins, R. Eds., Wiley-Interscience: New York,* 1988.
24 E. Posnjak, *J. Phys. Chem.,* 1926, **30**(8), 1073
25 V. G. Kessler, Single Source Precursor Approach - Hydrolysis Mechanisms in Organic Media, in Chemical Solution Deposition of Functional Oxide Thin Films, Eds. T. Schneller, R. Waser, M. Kosec, D. Payne, *Springer, Dordrecht*, 2013, 71-92.
26 V. G. Kessler, G. I. Spijksma, G. A. Seisenbaeva, S. Håkansson, D. H. A. Blank and H. J. M. Bouwmeester, *J. Sol-Gel Sci. Technol.,* 2006, **40**, 163.
27 G. A. Seisenbaeva and V. G. Kessler, *Nanoscale*, 2014, **6**, 6229.
28 A. F. Shihada, A. S. Abushamleh and F. Weller, *Anorg. Allg. Chem.,* 2004, **630**, 841.
29 J. A. Toledo-Antonio, R. Gutierrez-Baez, P. J. Sebastian, and A. Vazquez, *J. Solid State Chem.*, 2003, **174**, 241.
30 W. H. Baur and A. A. Khan, *Acta Crystallogr., Sect. B*, 1971, **27**, 2133.
31 W. H. Baur, *Acta Crystallogr.*, 1956, **9**, 515.
32 T. Yamanaka, R. Kurashima nad J. Mimaki, *Z. Kristallogr.,* 2000, **215**, 424.
33 B. Grzeta, E. Tkalcec, C. Goebbert, M. Takeda, M. Takahashi, K. Nomura and M. Jaksic, *J. Phys. Chem. Solids*, 2002, **63**, 765.
34 G. J. McCarthy and J. M. Welton, *Powder Diffr.*, 1989, **4**, 156.
35 G. A. Seisenbaeva, G. Daniel, J. M. Nedelec, Y. K. Gun'ko, V.G. Kessler, *J. Mater. Chem*., 2012, **22**, 20374-20380.
36 M. Volmer and A. Weber, *Z. Physikal. Chemie*, 1925, **119**, 277.
37 L. Li, F. Zong, X. Cui, H. Ma, X. Wu, Q. Zhang, Y. Wang, F. Yang and J. Zhao, *Mater. Lett.*, 2007, **61**, 4152.
38 D. Chen and L. Gao, *J. Colloid Interface Sci.*, 2004, **279**, 137.
39 N. Noor and I. P. Parkin, *Thin Solid Films*, 2013, **532**, 26.
40 A. Diéguez, A. Romano-Rodríguez, A. Vilà, and J. R. Morante, *J. Appl. Phys.*, 2001, **90**, 1550-1557.
41 N.Y. Turova, E.P. Turevskaya, V.G. Kessler, M.I. Yanovskaya, The Chemistry of Metal Alkoxides, Kluwer AP, Boston, 2002.
42 V. Etacheri, G.A. Seisenbaeva, J. Caruthers, G. Daniel, J.M. Nedelec, V.G. Kessler, V.G. Pol, *Adv Energy Mater.,* 2015, **5**, 1401289, 1-8.
43 G. A. Seisenbaeva, M. P. Moloney, R. Tekoriute, A. Hardy-Dessources, J. M. Nedelec, Y. K. Gun'ko, V. G. Kessler, *Langmuir*, 2010, **26**, 9809.
44 K. N. Yu, Y. Xiong, Y. Liu and C. Xiong, *Phys. Rev. B: Condens. Matter Mater. Phys.*, 1997, **55**, 2666.
45 A. Diéguez, A. Romano-Rodríguez, A. Vilà and J.R. Morante, *J. Appl. Phys.*, 2001, **90**, 1550.
46 Z. Chen, J. Lai, and C. Shek, *Phys. Rev. B: Condens. Matter Mater. Phys.,* 2004, **70**, 165314.
47 R. S. Katiyar, P. Dawson, M. M. Hargreave, and G. R. Wilkinson, *J. Phys. C: Solid State Phys.*, 1971, **4**, 2421.
48 A. Kar, J. Yang, M. Dutta, M. A. Stroscio, J. Kumari, M. Meyyappan, *Nanotechnology*, 2009, **20**, 065704.
49 C. Drake, S. Deshpande and S. Seal, *Appl. Phys. Lett.*, 2006, 89, 143116.
50 M. Melle-Franco and G. Pacchioni, *Surface Sci.*, 2000, **461(1–3)**, 54.
51 A. Rosenthal, A. Tarre, A. Gerst, J. Sundqvist, A. Harsta, A. Aidla, J. Aarik, V. Sammelselg, T. Uustare, *Sens. Actuators, B*, 2003, **93**, 552.
52 B.-K. Min and S.-D. Choi, *Sens. Actuators, B*, 2004, **98**, 239.
53 M. Choudhary, V. N. Mishra and R. Dwivedi, *J. Electron. Mater.*, 2013, **42**, 2793.